CHEMISTRY OF MATERIALS

Article

pubs.acs.org/cm

Solution-Processed Graphite Membrane from Reassembled Graphene Oxide

Titisa Ghosh,[†] Chandan Biswas,[‡] Joonsuk Oh,[§] Girish Arabale,[†] Taeseon Hwang,[§] Nguyen Dang Luong,[§] Meihua Jin,[¶] Young Hee Lee,[†,¶] and Jae-Do Nam*[,†,§]

[†]Department of Energy Science, [‡]Sungkyunkwan Advanced Institute of Nanotechnology, [§]Department of Polymer Science and Engineering, and [¶]Department of Physics, Sungkyunkwan University, Suwon, South Korea

Supporting Information

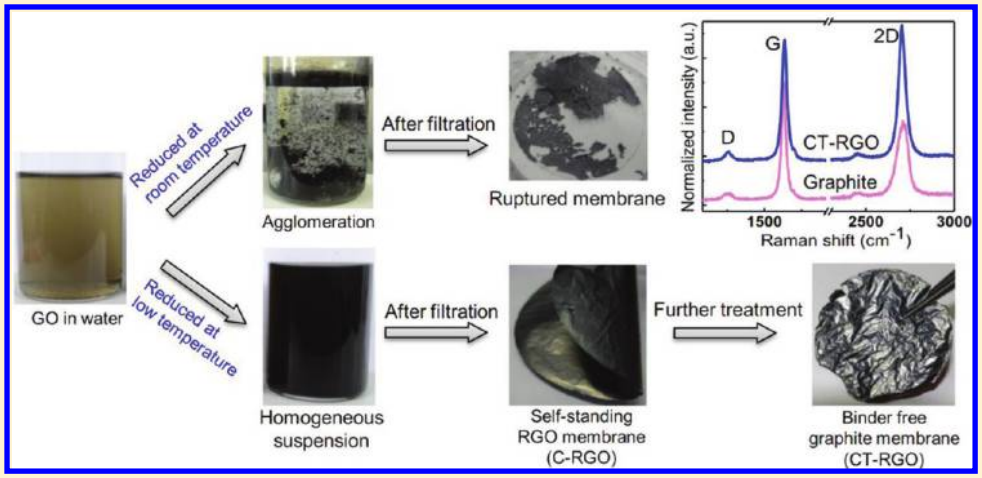

ABSTRACT: A new synthesis route of a solution-processed highly conductive self-standing graphite membrane from reassembled graphene oxide (GO) has become one of the intensive research focus, because of its immense application opportunities. Previously demonstrated techniques were limited by the unstable reduced graphene oxide (RGO) dispersion and agglomeration during chemical reduction without any surfactant. This results in poor packing morphology and low electrical conductivity of the RGO membrane. Here, we report a novel synthesis route of a highly concentrated RGO solution from exfoliated GO, which results highly conductive and self-standing RGO membrane without using any binders or organic solvents. Our low-temperature reduction method is significantly different from previous investigations in which controlling the reduction rate by lowering the reduction temperature of the GO solution and collision probability was the key factor in preventing random agglomeration. Further high-temperature reduction of the RGO membrane gave rise to a reassembled graphite structure containing negligible oxygen content (O 1s/C 1s = 0.005), and high electrical conductivity (up to 1.6×10^5 S/m) without disintegration of its self-standing feature. This result is better than any previously reported value. Developed RGO membrane could be mass-produced for various flexible device applications. The in-plane alignment and through-thickness consolidation of GO and RGO membranes using vacuum-filtration and thermal treatment successfully ensured the synthesis of highly conductive, mechanically robust RGO and graphite membranes.

KEYWORDS: *graphite, reduced graphene oxide, graphite membrane, self-standing, binder free*

INTRODUCTION

A stable suspension of GO can be obtained by ultrasonic treatment of graphite oxide in water.[1,2] Extensive effort has been made for the development of reassembled RGO (from GO) membranes through various techniques,[3−6] such as amine-functionalized graphene oxide paper,[7] vapor-phase-reduced graphene oxide (V-RGO) paper,[8] multilayered stacked graphene oxide film,[9] high-temperature annealing,[10] and combination of hydrazine vapor and high-temperature annealing.[10,11] However, these techniques are limited by poor packing morphology and low electrical conductivity, because of difficulties in achieving a stable RGO dispersion and the presence of numerous lattice defects and spatial interruptions from various oxygen groups. The RGO membranes reduced by hydrazine solution have been reported to have a sheet resistance of 10^5−10^7 Ω/sq, which contain localized fragmentation of RGO.[10] Alternatively, hydrazine vapor has been used for GO reduction, but it could only reduce the exposed outer layer of GO film in the vapor-phase reduction.[9] Chemical reduction of GO solution using a reducing agent such

Received: November 14, 2011
Revised: December 30, 2011
Published: December 31, 2011

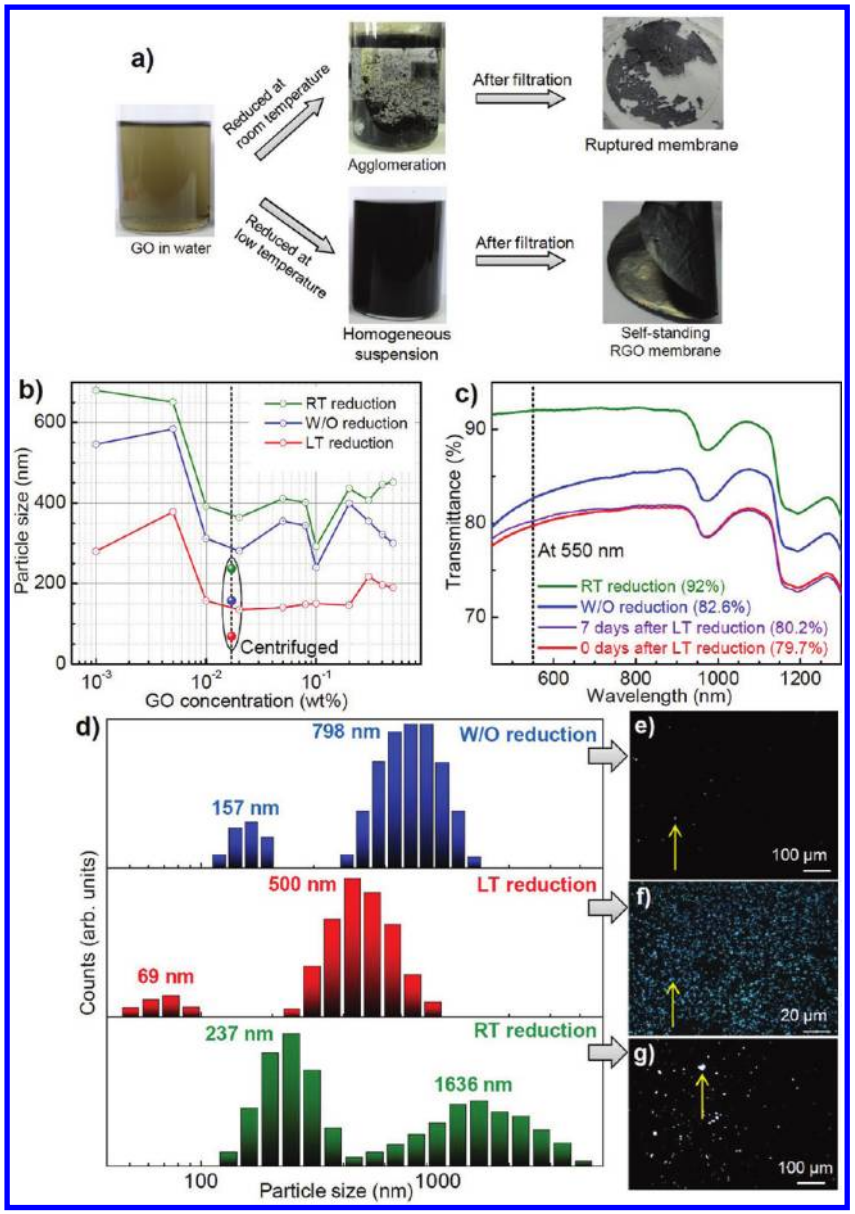

Figure 1. (a) Schematic representation of reaction-rate-controlled reduction methods. Reduction of dispersed GO solution without controlling the reaction temperature produces agglomeration of RGO, whereas temperature-controlled reduction reaction produces homogeneous, stable suspension, resulting in uniform large area self-standing RGO membrane after filtration. (b) Dynamic light scattering (DLS) measurements of the particle distributions of without reduced (W/O), low-temperature (LT) reduced, and room-temperature (RT) reduced GO solutions with different GO concentrations (solutions were measured without centrifugation and precipitation) in water. Centrifuged GO solution designated with solid dots containing fixed GO concentration. (c) Transmission microscopic analysis of RT, W/O, and LT GO solution after reduction compared with preservation under ambient conditions for 7 days. (d) Particle size distributions of the centrifuged RT, W/O, and LT GO solutions. (e–g) Dark-field optical microscopic images of the dissolved particles in solution phase, before reduction, after LT reduction, and after RT reduction, respectively.

as hydrazine usually produces agglomeration, because of the unstable RGO solution, which cannot be filtered as a self-standing, large-area membrane. In this study, we report that a chemically reduced RGO membrane (with a sheet resistance of 11 Ω/sq and an electrical conductivity of 5.8×10^4 S/m) is much superior to the membrane synthesized by the V-RGO method. This result is better than any previous reported results.[9−12] Homogeneous and stable suspension of RGO in water without using any binder and/or surfactant has been achieved by lowering the reaction rate of the reduction process in the first step of reduction, which is significantly different from previous reports. This produces a highly conductive self-standing, binder-free graphite membrane that previously was not demonstrated. Furthermore, Raman spectroscopy and X-ray photoelectron spectroscopy (XPS) demonstrate negligible oxygen content (O 1s/C 1s ratios up to 0.005) of the synthesized RGO membrane, which is almost similar to that of graphite.

EXPERIMENTAL SECTION

Material Preparation. GO was prepared using a modified Brodie method developed previously.[13] Five grams (5 g) of graphite flakes (Sigma−Aldrich) was added to a mixture containing 45 mL of concentrated nitric acid and 87.5 mL of sulfuric acid in an ice bath. Twenty grams (20 g) of potassium chlorate was slowly added to the mixture over 1 h to avoid

dx.doi.org/10.1021/cm2033838 | Chem. Mater. 2012, 24, 594−599

sudden increases in temperature.[14] The synthesized GO was dispersed in deionized (DI) water with sonication for 3 h, followed by centrifugation at 4000 rpm for 15 min to remove any unexfoliated graphite oxide flakes. Preparation of high-quality chemically reduced graphene oxide (C-RGO) films was carried out by controlling the reaction rate. GO solution was kept at 2−5 °C, followed by the addition (dropwise) of 5 mM hydrazine solution. RGO membrane was prepared by vacuum filtration method from the above mixture, followed by drying at 70 °C for 5 h. Vapor-reduced graphene oxide films was prepared by reducing the GO membrane with hydrazine vapor at room temperature.[15] Thermally reduced graphene oxide (T-RGO) films were prepared by reducing GO membrane at high temperature. An elaborate description and process scheme of the synthesis methods was provided in the Supporting Information (Figure S1). GO films were annealed under vacuum conditions (1.25×10^{-6} Torr) at 1900 °C for 2 h. Chemically and thermally reduced graphene oxide (CT-RGO) films were prepared by further thermal reduction of C-RGO films under similar vacuum annealing conditions. The temperature profile of the low-temperature reduction process was discussed in Figure S2 in the Supporting Information.

Characterization. The morphology of the samples was characterized by field-emission scanning electron microscopy (JEOL, Model JSM 7000F) and transmission electron microscopy (JEOL, Model JEM 2100-2100F) at 200 kV. XPS analysis (QUANTUM 2000, Physical Electronics, USA) was performed using focused monochromatized Al Kα radiation (1486.6 eV) in order to determine changes in the atomic ratios of oxygen to carbon and the existence of functional groups. The sheet resistance of all our samples was measured by a four-point probe method (Keithley, Model 2000 multimeter) at room temperature. Raman spectroscopy (Renishaw, RM-1000 Invia) with excitation energy of 2.41 eV (514 nm, Ar^+ ion laser) was used to characterize the optical properties of our entire sample. The optical microscopy of the GO particles was carried out by an inverted optical microscope (AF6000B, Leica, Germany) combined with a high-resolution condenser (Cytoviva, Inc., Auburn, AL, USA) under dark-field conditions.[16] The average size of the particles dispersed in solution phase was measured by an ELS-8000 (Photal, Otsuka Electronics Co.) at a wavelength of 633 nm with a He−Ne laser as a light source using a square cell for dynamic light scattering (DLS) mode. The time-dependent autocorrelation function of the scattered light intensity was measured at a scattering angle of 60° at room temperature. The DLS measurements were repeated at least three times, and the average values were reported. Ultraviolet−visible−near-infrared (UV-vis-NIR) absorption spectroscopy was performed using a Cary 5000 spectrophotometer (Varian, Santa Clara, CA, USA).

RESULTS AND DISCUSSIONS

Low-Temperature Reduction Method. Stable RGO solution (up to 1 wt % of RGO concentration) in water was achieved by lowering the reduction temperature down to 0−5 °C, followed by a gradual temperature increment (up to ca. 100 °C). Room-temperature reduction resulted in rapid RGO agglomeration, as seen in Figure 1a. The stable RGO suspension provided a binder-free highly conductive RGO membrane, which could be obtained by stacking the GO sheets in the in-plane direction using a vacuum filtration method. In contrast, the room-temperature reduced RGO suspension could not make a self-standing membrane.

The particle size distributions in without reduced GO (W/O), LT-reduced RGO, and RT-reduced RGO solutions can be clearly compared using dynamic light scattering (DLS) analysis (Figure 1b), as a function of GO concentration in water. These measurements clearly show that the particle size in GO (W/O) solution increased after RT reduction, whereas it was significantly reduced by LT reduction. The decrement of RGO particle size due to the reduction of collision probability at low reaction temperature resulted in a stable RGO suspension. DLS results support the visual examination in Figure 1a, as the increased particle size attributes to the partial agglomeration. The particle sizes marked (as circle) in Figure 1b show the DLS results after centrifugation of 1 wt % GO solutions at 4000 rpm for 15 min. It can be seen that the particle sizes in centrifuged solutions were substantially decreased, compared to noncentrifuged samples (maintaining the same trend), which may ensure a stable RGO solution.

The long-time stability of these RGO solutions was examined using transmittance spectroscopy in Figure 1c after 7 days of storage. The stable GO solution (W/O) exhibited 82.6% transmittance at a wavelength of 550 nm before reduction. The RT reduction method resulted in rapid agglomeration and precipitation, leaving a clear solution, as represented by 92% transmittance. However, the LT reduction method resulted in a substantial decrease in transmittance at 80%, corresponding to a well-dispersed, stable RGO solution. In particular, the LT solution after 7 days of storage showed the same transmittance as the pristine one. Figure 1d shows the particle size distributions of the solutions prepared by the W/O (GO), RT, and LT methods. All the samples exhibit bimodal particle size distributions. The particle size of the RT method (Figure 1g) was larger than that of the W/O (Figure 1e) and LT methods (Figure 1f); this was verified by the dark-field optical microscopic images. This clearly validates the fact that our LT reduction method gives smaller RGO particle sizes than GO or RGO prepared by the RT method. The stable RGO suspension produced at lower temperatures plays a key role in the preparation of a highly concentrated stable RGO solution, which subsequently allows fabrication of free-standing, highly conductive, and large-area membranes.

Material Study. By filtering and drying the GO (W/O) and LT suspensions, the self-standing membranes were successfully fabricated. Figures 2a and 2b compare the XPS broad scan spectra of the GO (W/O) and C-RGO (LT) membranes with high-resolution narrow scan analyses in the carbon region (inset), respectively. It can be clearly seen that the oxygen functional groups in C-RGO were substantially decreased by the rate-controlled reduction method. We compared our C-RGO with V-RGO, because the V-RGO method is most commonly used. Our C-RGO (Figure 2b) and V-RGO membranes (Figure S3a in the Supporting Information) both showed lower peak intensities of oxygen functional groups than those in the GO membrane (Figure 2a). However, the atomic ratio of oxygen to carbon (O 1s/C 1s) of C-RGO (0.3) was significantly lower than that of V-RGO (0.59), demonstrating that our LT reduction method provides higher efficiency of oxygen removal.

An additional peak observed at 285.6 eV corresponding to a C−N bond appeared for the V-RGO (Figure 2c) and C-RGO (Figure 2d) samples after reduction by hydrazine, in which the partial reduction of carbonyl functionalities occurs to form hydrazone ($R_1R_2C{=}NNH_2$) groups.[10] However, the narrow scan N 1s XPS spectrum of V-RGO (Figure 2c) displayed a

dx.doi.org/10.1021/cm2033838 | Chem. Mater. 2012, 24, 594−599

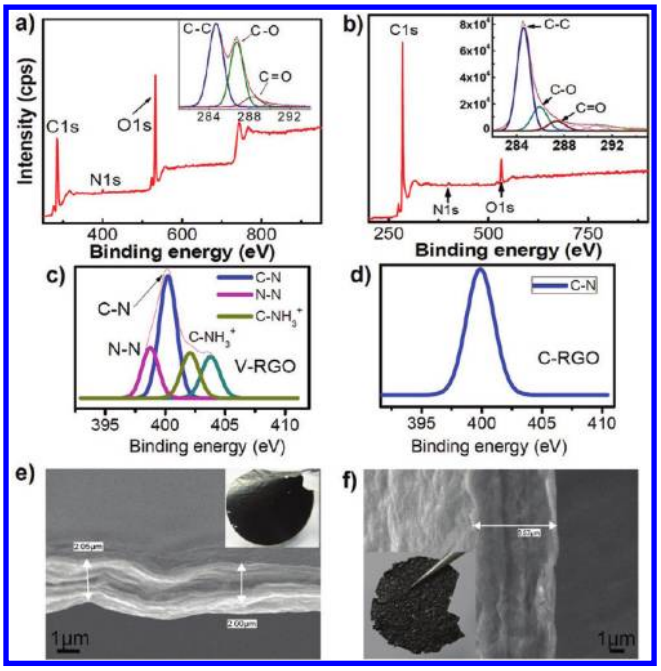

Figure 2. (a) XPS wide scan and deconvoluted C 1s spectra (inset) of GO. (b) XPS wide scan and deconvoluted C 1s spectra (inset) of C-RGO. (c) High-resolution XPS narrow scans of the N 1s region of V-RGO membrane. (d) High-resolution XPS narrow scans of the N 1s region of C-RGO membranes. (e) FE-SEM and digital camera (inset) images of C-RGO. (f) FE-SEM and digital camera (inset) images of V-RGO.

peak at ~398 eV (assigned to N–N),[17] corresponding to residual hydrazine, which was not the case with C-RGO (Figure 2d). Moreover, the O 1s/C 1s ratio observed in the C-RGO samples (0.06) was much lower than that of V-RGO (0.12), suggesting higher reduction capabilities provided by our low-temperature reduction method. Furthermore, residual N species contamination was significantly reduced in the C-RGO (0.53 at. %) samples, compared to the V-RGO (2.06 at. %) samples. Figures 2e and 2f present scanning electron microscopy (SEM) cross-sectional images of membranes obtained by the C-RGO (Figure 2e) and V-RGO (Figure 2f) methods. Our C-RGO samples (Figure 2e) revealed well-packed layers throughout the entire cross section, but rough surfaces with bubbles were clearly visible in the V-RGO samples (Figure 2f). These results clearly indicate that chemical reduction with hydrazine vapor is less efficient than our C-RGO method.

In this study, thermal treatments (at 1900 °C) were employed for the complete reduction of GO (W/O) and C-RGO membranes using different methods: (i) thermal reduction of GO to synthesis "T-RGO" membrane and (ii) thermal reduction of C-RGO to synthesis "CT-RGO" membrane. As seen in Table 1 and Figure 3, thermal treatment of the above samples exhibited further removal of the oxygen functionalized group, reaching 0.57 at. % in CT-RGO and 0.8 at. % in T-RGO, which were significantly lower than 5.8 at. % in C-RGO and 25.3 at. % in GO, respectively (see Figure S5 in the Supporting Information). Significantly, the oxygen functional group measured in the CT-RGO samples (0.57 at. %) showed an even lower value than that of commercial pristine graphite flakes (2.8 at.%; see Figures S3b and S5 in the Supporting Information, as well as Table 1). Furthermore, the O 1s/C 1s

Table 1. List of Atomic Composition of Graphite, Graphene Oxide, C-RGO, V-RGO, T-RGO, and CT-RGO

sample name	description	C (at. %)	O (at. %)	N (at. %)	O/C ratio
graphite	flake	97.02	2.899		0.029
graphite oxide	modified Brodie method	73.73	25.38		0.344
C-RGO	low temperature	93.67	5.796	0.533	0.061
V-RGO	reduced by vapor	87.39	10.54	2.058	0.12
T-RGO	annealed at 1900 °C	99.15	0.844		0.008
CT-RGO	annealed at 1900 °C	99.43	0.566		0.005

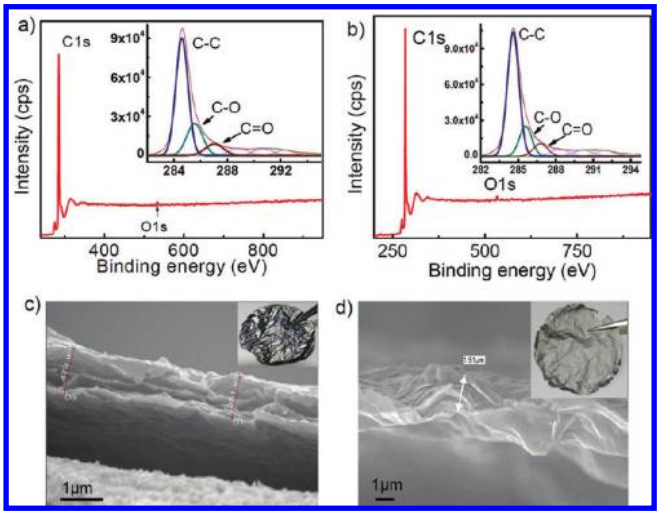

Figure 3. (a) XPS wide scan and deconvoluted C 1s spectra (inset) of CT-RGO. (b) XPS wide scan and deconvoluted C 1s spectra (inset) of T-RGO. (c) FE-SEM and digital camera (inset) images of CT-RGO self-sanding membrane. (d) FE-SEM and digital camera (inset) images of T-RGO membrane.

ratio of CT-RGO at 0.005 strongly suggests complete oxygen reduction in the GO samples. The SEM images of the CT-RGO and T-RGO membranes can be seen in Figures 3c and 3d, respectively. After thermal treatment, the surface of CT-RGO turned smoother and shiny metallic, with decreased thicknesses from 2.05 μm to 1.48 μm. This could be attributed from the removal of O and N atoms, resulting in interlayer consolidation of graphene sheets. Additional surface morphologies can be seen in Figures S4 and S6 in the Supporting Information.

In Raman spectra, a D-band at 1340 cm^{-1} and a broad G-band at 1580 cm^{-1} can be seen in Figure 4a, similar to the previous observations.[18] The prominent D-peak evolved from the structural imperfections created by the attachment of hydroxyl and epoxide groups on the carbon basal plane.[19] The G-band occurred at 1581 cm^{-1}, which corresponds to the recovery of the hexagonal network of C atoms with defects.[19] The I_D/I_G ratio of C-RGO increased notably, indicating that the reduction process altered the structure of GO[19] with a high quantity of structural defects. The intensities of the two-dimensional (2D ≈ 2694 cm^{-1}) and S3 (~2910 cm^{-1}) peaks in C-RGO increased more significantly than those of V-RGO, demonstrating increased graphitization. Figure 4b shows the degrees of graphitization after thermal treatment between graphite, C-RGO, TRGO, and CT-RGO. Significant reduction in the I_D/I_G ratio from 1.26 to 0.15 for the C-RGO and CT-RGO samples, respectively, was strongly observed, suggesting

dx.doi.org/10.1021/cm2033838 | Chem. Mater. 2012, 24, 594–599

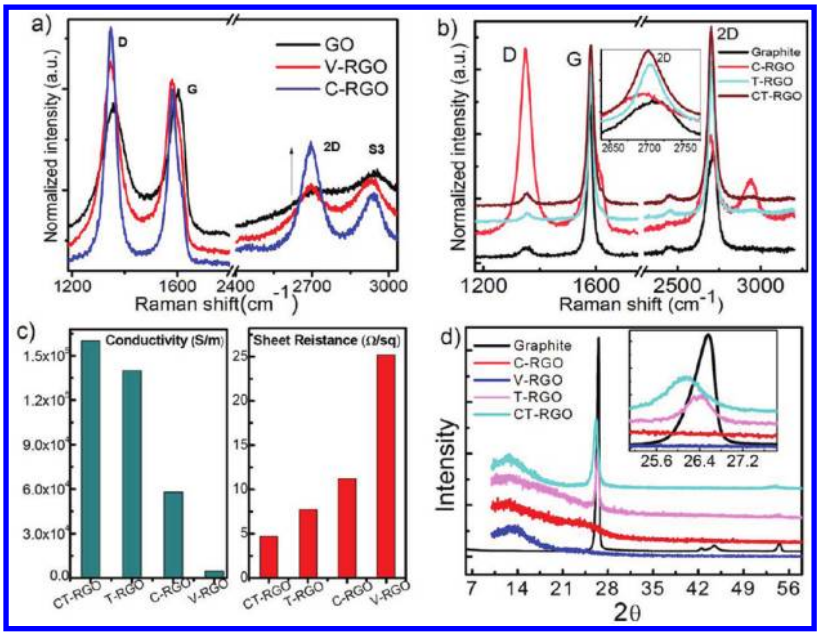

Figure 4. (a) Raman spectra of GO, V-RGO, and C-RGO. (b) Raman spectra of graphite, C-RGO, T-RGO, and CT-RGO samples. (c) Sheet resistance and conductivity comparisons of CT-RGO, T-RGO, C-RGO, and V-RGO membranes. (d) XRD patterns of graphite, C-RGO, V-RGO, T-RGO, and CT-RGO samples.

that the crystal defects were substantially reduced and graphitization successfully achieved in the CT-RGO samples. This was also supported by the increased 2D peak (near 2700 cm^{-1}) in CT-RGO.

Figure 4c compares the electrical properties of the RGO membranes fabricated by different methods. The GO (or W/O) membrane had a sheet resistance and conductivity of 1 MΩ/sq and 0.13 S/m, respectively (Table 2). An increase in the relative amount of C 1s/O 1s ratio usually causes a significant decrease in sheet resistance[10−12,20] and an increased work function of the reduced graphene oxide membranes.[20] It has been reported that the sheet resistance of V-RGO is often influenced by the effective reduction depth (d_e), since hydrazine-vapor reduction usually reduces the outer layer of the V-RGO membrane,[21] limiting overall sheet resistance. Accordingly, our C-RGO showed lower sheet resistance (11.2 Ω/sq) and higher conductivity (5.8×10^4 S/m) than those of V-RGO (25.9 Ω/sq, 4.6×10^3 S/m) due to greater amount of oxygen and nitrogen elements.[17] The electrical conductivity of reduced graphene oxide sheets increases with an increasing amount of reducing agent and tapers off when the C/O ratio exceeds a specific value.[10] After thermal treatment, the electrical conductivity (sheet resistance) substantially increased (decreased) from 5.8×10^4 S/m of C-RGO to 1.6×10^5 S/m of CT-RGO (from 11.2 Ω/sq to 4.7 Ω/sq) due to the elimination of almost all oxygen and nitrogen functionalities and effective interlaminar consolidation. Although T-RGO samples displayed improved electrical conductivity and sheet resistance compared to GO membrane, CT-RGO was much better than T-RGO membrane. Note that the electrical conductivity of our C-RGO membrane (5.8×10^4 S/m) is the highest yet, and CT-RGO (1.6×10^5 S/m) closely approaches pristine graphite.

Table 2. Comparison of Listed Membrane Thicknesses and the Electrical Properties of Graphite Oxide, C-RGO, V-RGO, T-RGO, and CT-RGO Membranes

sample name	description	conductivity (S/m)	sheet resistance (Ω/sq)	thickness (μm)
graphite oxide	modified Brodie method	0.13	1×10^6	8
C-RGO	low temperature	5.8×10^4	11.2	1.53
V-RGO	reduced by vapor	4.6×10^3	25.9	8.57
T-RGO	annealed at 1900 °C	1.4×10^5	7.7	1.51
CT-RGO	annealed at 1900 °C	1.6×10^5	4.7	1.35

Figure 4d shows high resolution X-ray diffraction (XRD) pattern comparing graphite, C-RGO, V-RGO, T-RGO, and CT-RGO membranes. A typical broad peak near 12° (d-spacing ≈ 7.31 Å) was observed for both C-RGO and V-RGO membranes, which can be attributed to the expansion of the 3.4 Å spacing between typical graphene sheets to accommodate the water molecules trapped between the oxygen-containing functional groups.[3,22] After thermal treatment, the XRD pattern of CT-RGO showed a sharp peak at 26.23° (d-spacing ≈ 3.39 Å), which corresponds to the characteristic peak of pristine graphite at $2\theta = 26.5°$ (d-spacing ≈ 3.35 Å). This demonstrates that a graphite-like membrane can be fabricated from a stabilized RGO solution through a rate-controlled reduction and thermal treatment. It should also be mentioned that the in-plane alignment and through-thickness consolidation of the RGO sheets are keys for the fabrication of a highly conductive and self-standing membrane.

■ CONCLUSIONS

Here, we report a novel method to prepare a stabilized RGO solution at a reduced reduction rate. Our chemically reduced RGO (or C-RGO) solution allowed the fabrication of self-standing RGO membranes aligned in the in-plane direction with excellent interlaminar consolidation. After thermal treatment of the C-RGO membrane up to 1900 °C, the resulting CT-RGO membrane gave a graphite-like structure and electrical properties. The developed methodology allows a

dx.doi.org/10.1021/cm2033838 | Chem. Mater. 2012, 24, 594−599

simple and large-volume production of RGO and graphite papers with excellent electrical properties.

■ ASSOCIATED CONTENT

Supporting Information

Containing supporting data, text, and figures. This material is available free of charge via the Internet at http://pubs.acs.org.

■ AUTHOR INFORMATION

Corresponding Author

*E-mail: jdnam@skku.edu.

■ ACKNOWLEDGMENTS

This research was supported by WCU (World Class University) program through the Korea Science and Engineering Foundation funded by the Ministry of Education, Science and Technology (No. R31-2008-000-10029-0). The authors also acknowledge the instrumental and technical support provided by the GRRC program from Gyeonggi Province.

■ REFERENCES

(1) Stankovich, S.; Dikin, D. A.; Piner, R. D.; Kohlhaas, K. A.; Kleinhammes, A.; Jia, Y.; Wu, Y.; Nguyen, S. T.; Ruoff, R. S. *Carbon* **2007**, *45*, 1558−1565.

(2) Gilje, S.; Han, S.; Wang, M.; Wang, K. L.; Kaner, R. B. *Nano Lett.* **2007**, *7*, 3394−3398.

(3) Dikin, D. A.; Stankovich, S.; Zimney, E. J.; Piner, R. D.; Dommett, G. H. B.; Evmenenko, G.; Nguyen, S. T.; Ruoff, R. S. *Nature* **2007**, *448*, 457−460.

(4) Xu, Y.; Bai, H.; Lu, G.; Li, C.; Shi, G. *J. Am. Chem. Soc.* **2008**, *130*, 5856−5857.

(5) Li, D.; Muller, M. B.; Gilje, S.; Kaner, R. B.; Wallace, G. G. *Nat. Nano* **2008**, *3*, 101−105.

(6) Chen, H.; Müller, M. B.; Gilmore, K. J.; Wallace, G. G.; Li, D. *Adv. Mater.* **2008**, *20*, 3557−3561.

(7) Compton, O. C.; Dikin, D. A.; Putz, K. W.; Brinson, L. C.; Nguyen, S. T. *Adv. Mater.* **2010**, *22*, 892−896.

(8) Moon, I. K.; Lee, J.; Ruoff, R. S.; Lee, H. *Nat. Commun.* **2010**, *1*, 73.

(9) Liu, J.; Lin, Z.; Liu, T.; Yin, Z.; Zhou, X.; Chen, S.; Xie, L.; Boey, F.; Zhang, H.; Huang, W. *Small* **2010**, *6*, 1536−1542.

(10) Becerril, H. A.; Mao, J.; Liu, Z.; Stoltenberg, R. M.; Bao, Z.; Chen, Y. *ACS Nano* **2008**, *2*, 463−470.

(11) Eda, G.; Fanchini, G.; Chhowalla, M. *Nat. Nano* **2008**, *3*, 270−274.

(12) Park, S.; An, J.; Piner, R. D.; Jung, I.; Yang, D.; Velamakanni, A.; Nguyen, S. T.; Ruoff, R. S. *Chem. Mater.* **2008**, *20*, 6592−6594.

(13) Staudenmaier, L. *Ber. Dtsch. Chem. Ges.* **1898**, *31*, 1481.

(14) McAllister, M. J.; Li, J.-L.; Adamson, D. H.; Schniepp, H. C.; Abdala, A. A.; Liu, J.; Herrera-Alonso, M.; Milius, D. L.; Car, R.; Prud'homme, R. K.; Aksay, I. A. *Chem. Mater.* **2007**, *19*, 4396.

(15) Yang, D.; Velamakanni, A.; Bozoklu, G.; Park, S.; Stoller, M.; Piner, R. D.; Stankovich, S.; Jung, I.; Field, D. A.; Ventrice, C. A. Jr.; Ruoff, R. S. *Carbon* **2009**, *47*, 145.

(16) Vainrub, A.; Pustovyy, O.; Vodyanoy, V. *Opt. Lett.* **2006**, *31*, 2855.

(17) Ren, H.; Li, Q.; Su, H.; Shi, Q. W.; Chen, J.; Yang, J. L. arXiv.org e-Print archive 2007, http://arxiv.org/abs/0711.1700.

(18) Pimenta, M. A.; Dresselhaus, G.; Dresselhaus, M. S.; Cancado, L. G.; Jorio, A.; Saito, R. *Phys. Chem. Chem. Phys.* **2007**, *9*, 1276−1290.

(19) Cancado, L. G.; Takai, K.; Enoki, T.; Endo, M.; Kim, Y. A.; Mizusaki, H.; Jorio, A.; Coelho, L. N.; Magalhaes-Paniago, R.; Pimenta, M. A. *Appl. Phys. Lett.* **2006**, *88*, 163106.

(20) (a) Shin, H.-J.; Kim, K. K.; Benayad, A.; Yoon, S.-M.; Park, H. K.; Jung, I.-S.; Jin, M. H.; Jeong, H.-K.; Kim, J. M.; Choi, J.-Y.; Lee, Y. H. *Adv. Funct. Mater.* **2009**, *19*, 1987−1992. (b) Sreeprasad, T. S.; Samal, A. K.; Pradeep, T. *J. Phys. Chem. C* **2009**, *113*, 1727−1737.

(21) Tung, V. C.; Chen, L.-M.; Allen, M. J.; Wassei, J. K.; Nelson, K.; Kaner, R. B.; Yang, Y. *Nano Lett.* **2009**, *9*, 1949−1955.

(22) Park, S.; Lee, K.-S.; Bozoklu, G.; Cai, W.; Nguyen, S. T.; Ruoff, R. S. *ACS Nano* **2008**, *2*, 572−578.